

## Computing induced charges in inhomogeneous dielectric media: Application in a Monte Carlo simulation of complex ionic systems

Dezső Boda,<sup>1</sup> Dirk Gillespie,<sup>2,3,\*</sup> Wolfgang Nonner,<sup>3</sup> Douglas Henderson,<sup>4</sup> and Bob Eisenberg<sup>2</sup><sup>1</sup>*Department of Physical Chemistry, University of Veszprém, P.O. Box 158, Veszprém, Hungary*<sup>2</sup>*Department of Molecular Biophysics and Physiology, Rush University Medical Center, Chicago, Illinois 60612, USA*<sup>3</sup>*Department of Physiology and Biophysics, University of Miami School of Medicine, Miami, Florida 33101, USA*<sup>4</sup>*Department of Chemistry and Biochemistry, Brigham Young University, Provo, Utah 84602, USA*

(Received 12 November 2003; revised manuscript received 16 December 2003; published 29 April 2004)

The efficient calculation of induced charges in an inhomogeneous dielectric is important in simulations and coarse-grained models in molecular biology, chemical physics, and electrochemistry. We present the *induced charge computation* (ICC) method for the calculation of the polarization charges based on the variational formulation of Allen *et al.* [Phys. Chem. Chem. Phys. **3**, 4177 (2001)]. We give a different solution for their extremum condition that produces a matrix formulation. The induced charges are directly calculated by solving the linear matrix equation  $A\mathbf{h}=\mathbf{c}$ , where  $\mathbf{h}$  contains the discretized induced charge density,  $\mathbf{c}$  depends only on the source charges—the ions moved in the simulation—and the matrix  $A$  depends on the geometry of dielectrics, which is assumed to be unchanged during the simulation. Thus, the matrix need be inverted only once at the beginning of the simulation. We verify the efficiency and accuracy of the method by means of Monte Carlo simulations for two special cases. In the simplest case, a single sharp planar dielectric boundary is present, which allows comparison with exact results calculated using the method of electrostatic images. The other special case is a particularly simple case where the matrix  $A$  is not diagonal: a slab with two parallel flat boundaries. Our results for electrolyte solutions in these special cases show that the ICC method is both accurate and efficient.

DOI: 10.1103/PhysRevE.69.046702

PACS number(s): 02.70.Ns, 05.10.Ln

### I. INTRODUCTION

The continuing increase in computer speed and storage is making particle simulations more practical, but the strength and range of electrostatic interactions continue to pose formidable computational problems [1–4]. While it is possible to simulate more and more particles in atomic detail, regions of many systems are still modeled at low resolution. Such regions may be too large for detailed simulations or their properties may not be known in atomic detail. One type of coarse graining uses a spatially varying dielectric coefficient to describe the fast electronic, atomic, and molecular motions in polarizable materials. Dielectrics have often been used this way to model electrochemical interfaces [5–7] semiconductor junctions [8], the solvation of macromolecules such as DNA and proteins [9,10], cell membranes [11,12], and ion channels [13–28].

Even in idealized dielectric materials, determining the electrostatic potential  $\psi(\mathbf{r})$  is nontrivial when the dielectric coefficient  $\epsilon(\mathbf{r})$  is spatially inhomogeneous. The general solution to the problem is to solve the Poisson equation

$$-\epsilon_0 \nabla \cdot [\epsilon(\mathbf{r}) \nabla \psi(\mathbf{r})] = \rho(\mathbf{r}), \quad (1)$$

and boundary conditions, where  $\epsilon_0$  is the permittivity of free space and  $\rho(\mathbf{r})$  is the source charge density. However, for a three-dimensional system, solving this equation is computationally expensive, technically difficult, and, in particle simulations, generally a rate-limiting step [8]. For this rea-

son, the effects of boundary conditions and spatial variation of the dielectric coefficient are sometimes ignored.

In this paper we include an inhomogeneous dielectric coefficient in particle simulations by focusing on the polarization charges induced by the source charges in the system and *not* on the electrostatic potential. In this way, we deal with two sets of charges, the source charges and the induced charges, which (once calculated) can be treated in the calculations in much the same way as source charges. For example, in a Monte Carlo (MC) simulation of ions, the energy (including electrostatic energy) of the system is computed to determine the probability that a particle move is accepted. If induced charges are included in this calculation, the energy of the dielectric system can be determined with the same code used for the source charges.

We compute the induced charge using a method based on the work of Allen, Hansen, and Melchionna [29] who derived an elegant variational approach to the problem and then applied their formulation in molecular dynamics (MD) simulations of water permeation through nanopores in a polarizable membrane [30–32]. The functional chosen by Allen *et al.* is not the only formalism that can be used, however. In the pioneering work of Marcus [33], a polarization free energy functional was introduced and used later by Felderhof [34]. Free energy functionals are readily applicable in dynamical problems, such as macromolecule conformational changes and solvation [35–38], because they treat the polarization fields as virtual dynamic variables of the system [35,37] in conjunction with Car-Parrinello techniques [39]. Recently, Attard [40] has given the thermodynamic potential for charges in dielectric media with constrained polarization using the variational formulation of Marcus [33] and showed that during the approach to equilibrium its derivative yields the thermodynamic force acting on the constrained induced

\*Corresponding author. Email address: dirk\_gillespie@rush.edu

surface charges. In these studies, the dielectric boundaries are allowed to move, so these approaches are different from ours where the geometry is assumed to be unchanged during the simulation.

In this paper, we present a minimization of the functional of Allen *et al.* for dielectric boundaries that yields a matrix equation  $A\mathbf{h}=\mathbf{c}$  where  $\mathbf{h}$  is the vector of induced charges. This *induced charge computation* (ICC) method is general and can be applied to dielectric interfaces that are not sharp. For the particular case when the interface is sharp, the ICC method reduces to the *boundary element method* (BEM) used in apparent surface charge (ASC) calculations of solvation [41–43]. The practical importance of this matrix formulation is that the matrix  $A$  depends only on the geometry of the dielectric medium, so that it must be inverted only once at the beginning of the simulation if the geometry and dielectrics are fixed. Only the vector  $\mathbf{c}$  depends on the source charges in the system and therefore the induced charges can be obtained from a simple matrix/vector multiplication.

We apply this method to MC simulations of hard-sphere ions near dielectric boundaries. The results show that the ICC method is both efficient for particle simulations and accurate when compared to MC simulations computed with analytic electrostatic formulas.

## II. THEORY

### A. Variational formulation

The procedure presented in this paper is based on the variational formulation given by Allen *et al.* [29]. In this subsection we introduce the problem and outline their approach (keeping their notations). A clear and detailed presentation can be found in the original paper.

Consider a discrete or continuous charge distribution  $\rho(\mathbf{r})$  confined to a domain  $\mathcal{D}$  of volume  $V$  with a boundary  $\mathcal{S}$ . With the boundary condition that  $\psi(\mathbf{r})$  is specified on  $\mathcal{S}$ , the potential satisfies the Poisson equation in vacuum

$$\nabla^2\psi(\mathbf{r})=-\frac{\rho(\mathbf{r})}{\varepsilon_0} \quad (2)$$

everywhere in  $\mathcal{D}$ , where  $\varepsilon_0$  is the permittivity of the vacuum. The solution of the Poisson equation corresponds to the minimum of the functional [44]

$$I[\psi]=\frac{1}{2}\int_{\mathcal{D}}\nabla\psi\cdot\nabla\psi d\mathbf{r}-\int_{\mathcal{D}}g(\mathbf{r})\psi(\mathbf{r})d\mathbf{r}, \quad (3)$$

where  $g(\mathbf{r})=\rho(\mathbf{r})/\varepsilon_0$ . The minimal value  $-\varepsilon_0 I[\psi]$  is the electrostatic energy  $W$  of the charge distribution.

When the domain  $\mathcal{D}$  is a dielectric material with a local dielectric susceptibility  $\chi(\mathbf{r})$ , the polarization charge density induced by the source (or external) charge distribution  $\rho(\mathbf{r})$  is associated with the potential through

$$\rho_{pol}(\mathbf{r})=-\nabla\cdot\mathbf{P}(\mathbf{r})=\varepsilon_0\nabla\cdot[\chi(\mathbf{r})\nabla\psi(\mathbf{r})], \quad (4)$$

where  $\mathbf{P}(\mathbf{r})=-\varepsilon_0\chi(\mathbf{r})\nabla\psi(\mathbf{r})$  is the local polarization. The corresponding Poisson equation satisfied by the potential is

$$\nabla^2\psi(\mathbf{r})=-\frac{1}{\varepsilon_0}[\rho(\mathbf{r})+\rho_{pol}(\mathbf{r})], \quad (5)$$

and the corresponding functional is

$$I[\psi]=\frac{1}{2}\int_{\mathcal{D}}\nabla\psi\cdot\nabla\psi d\mathbf{r}-\int_{\mathcal{D}}\psi\left[g+\frac{1}{2}\nabla\cdot(\chi\nabla\psi)\right]d\mathbf{r}. \quad (6)$$

In order to express  $I[\psi]$  as a functional of the induced (polarization) charge density

$$h(\mathbf{r})=\frac{\rho_{pol}(\mathbf{r})}{\varepsilon_0}, \quad (7)$$

the potential is split into the ‘‘external’’ and the ‘‘induced’’ parts

$$\begin{aligned} \psi(\mathbf{r}) &= \psi_e(\mathbf{r}) + \psi_i(\mathbf{r}) \\ &= \int_{\mathcal{D}}G(\mathbf{r}-\mathbf{r}')g(\mathbf{r}')d\mathbf{r}' + \int_{\mathcal{D}}G(\mathbf{r}-\mathbf{r}')h(\mathbf{r}')d\mathbf{r}'. \end{aligned} \quad (8)$$

$G(\mathbf{r})$  is the Green’s function that satisfies

$$\nabla^2G(\mathbf{r}-\mathbf{r}')=-\delta(\mathbf{r}-\mathbf{r}'), \quad (9)$$

where  $\delta(\mathbf{r}-\mathbf{r}')$  is the Dirac delta function. The task is to determine the induced charge density  $h(\mathbf{r})$  for a given external charge density  $g(\mathbf{r})=\rho(\mathbf{r})/\varepsilon_0$  that satisfies Eq. (5), or, equivalently, minimizes Eq. (6). After substituting Eq. (8) into Eq. (6), Allen *et al.* [29] show that determining  $h(\mathbf{r})$  is equivalent to minimizing the functional

$$\begin{aligned} I_2[h] &= \frac{1}{2}\int_{\mathcal{D}}\int_{\mathcal{D}}h(\mathbf{r})h(\mathbf{r}')G(\mathbf{r}-\mathbf{r}')d\mathbf{r}'d\mathbf{r} \\ &\quad - \frac{1}{2}\int_{\mathcal{D}}\int_{\mathcal{D}}h(\mathbf{r}')G(\mathbf{r}-\mathbf{r}')\nabla\cdot(\chi\nabla\psi_e)d\mathbf{r}'d\mathbf{r} \\ &\quad - \frac{1}{2}\int_{\mathcal{D}}\int_{\mathcal{D}}h(\mathbf{r}')\psi_e(\mathbf{r})\nabla\cdot[\chi\nabla G(\mathbf{r}-\mathbf{r}')]d\mathbf{r}'d\mathbf{r} \\ &\quad - \frac{1}{2}\int_{\mathcal{D}}\int_{\mathcal{D}}\int_{\mathcal{D}}h(\mathbf{r}')h(\mathbf{r}'')G(\mathbf{r}-\mathbf{r}') \\ &\quad \times \nabla\cdot[\chi\nabla G(\mathbf{r}-\mathbf{r}'')]d\mathbf{r}''d\mathbf{r}'d\mathbf{r}. \end{aligned} \quad (10)$$

Allen *et al.* show that the extremum condition

$$\frac{\delta I_2[h]}{\delta h(\mathbf{r})}=0 \quad (11)$$

leads back to the constitutive relation  $\mathbf{P}(\mathbf{r})=-\varepsilon_0\chi(\mathbf{r})\nabla\psi(\mathbf{r})$ . They also show that the extremum is a minimum and that the value of  $I[h]$  at the minimum reduces to minus the electrostatic energy.

Allen *et al.* solved the variational problem (after discretization) with a steepest descent method. In the following section, we use a different method that produces a matrix equation that we apply to molecular simulations.

### B. Solution of the extremum condition

After some manipulations [29], the functional derivative in Eq. (11) simplifies to

$$\begin{aligned} \frac{\delta I_2}{\delta h(\mathbf{r})} &= \int_{\mathcal{D}} h(\mathbf{r}') G(\mathbf{r}-\mathbf{r}') d\mathbf{r}' - \int_{\mathcal{D}} G(\mathbf{r}-\mathbf{r}') \\ &\times \nabla_{\mathbf{r}'} \cdot [\chi(\mathbf{r}') \nabla_{\mathbf{r}'} \psi_e(\mathbf{r}')] d\mathbf{r}' - \int_{\mathcal{D}} \int_{\mathcal{D}} h(\mathbf{r}'') \\ &\times G(\mathbf{r}-\mathbf{r}') \nabla_{\mathbf{r}'} \cdot [\chi(\mathbf{r}') \nabla_{\mathbf{r}'} G(\mathbf{r}'-\mathbf{r}'')] d\mathbf{r}' d\mathbf{r}'' \end{aligned} \quad (12)$$

Using the definition of the Green's function [Eq. (9)], the Poisson equation of the source charges  $[\nabla^2 \psi_e(\mathbf{r}) = -\rho(\mathbf{r})/\epsilon_0]$ , and the relation

$$\nabla \cdot (f \nabla g) = \nabla f \cdot \nabla g + f \nabla^2 g, \quad (13)$$

we derive the following equation at the functional minimum:

$$\begin{aligned} &\int_{\mathcal{D}} h(\mathbf{r}') \left[ \epsilon(\mathbf{r}') G(\mathbf{r}-\mathbf{r}') - \int_{\mathcal{D}} G(\mathbf{r}-\mathbf{r}'') \right. \\ &\quad \left. \times \nabla_{\mathbf{r}''} \epsilon(\mathbf{r}'') \cdot \nabla_{\mathbf{r}''} G(\mathbf{r}''-\mathbf{r}') d\mathbf{r}'' \right] d\mathbf{r}' \\ &= \int_{\mathcal{D}} G(\mathbf{r}-\mathbf{r}') \nabla_{\mathbf{r}'} \epsilon(\mathbf{r}') \cdot \nabla_{\mathbf{r}'} \psi_e(\mathbf{r}') d\mathbf{r}' \\ &\quad - \frac{1}{\epsilon_0} \int_{\mathcal{D}} [\epsilon(\mathbf{r}') - 1] \rho(\mathbf{r}') G(\mathbf{r}-\mathbf{r}') d\mathbf{r}', \end{aligned} \quad (14)$$

where

$$\epsilon(\mathbf{r}) = 1 + \chi(\mathbf{r}). \quad (15)$$

This equation may be further simplified by considering  $F[h(\mathbf{r}'); \mathbf{r}]$ , which is both a *function* of  $\mathbf{r}$  and a *functional* of  $h(\mathbf{r}')$  as described by Eq. (14),

$$F[h(\mathbf{r}'); \mathbf{r}] = \int_{\mathcal{D}} h(\mathbf{r}') u(\mathbf{r}, \mathbf{r}') d\mathbf{r}' - v(\mathbf{r}), \quad (16)$$

where  $u(\mathbf{r}, \mathbf{r}')$  is the expression in square brackets in the integral on the LHS of Eq. (14), while  $v(\mathbf{r})$  is the RHS of Eq. (14). It is  $h(\mathbf{r}')$  that we need to determine under the constraint  $F(\mathbf{r})=0$  for all  $\mathbf{r}$ . Since  $F(\mathbf{r})$  is identically 0, it follows that, as a function of  $\mathbf{r}$ ,  $\nabla^2 F(\mathbf{r})=0$  for all  $\mathbf{r}$ . Thus, we have the relation

$$\int_{\mathcal{D}} h(\mathbf{r}') \nabla_{\mathbf{r}'}^2 u(\mathbf{r}, \mathbf{r}') d\mathbf{r}' = \nabla_{\mathbf{r}}^2 v(\mathbf{r}). \quad (17)$$

Applying this identity and Eq. (9) to Eq. (14) gives

$$\begin{aligned} h(\mathbf{r}) \epsilon(\mathbf{r}) - \int_{\mathcal{D}} h(\mathbf{r}') \nabla_{\mathbf{r}'} \epsilon(\mathbf{r}') \cdot \nabla_{\mathbf{r}'} G(\mathbf{r}-\mathbf{r}') d\mathbf{r}' \\ = \nabla_{\mathbf{r}} \epsilon(\mathbf{r}) \cdot \nabla_{\mathbf{r}} \psi_e(\mathbf{r}) - \frac{1}{\epsilon_0} [\epsilon(\mathbf{r}) - 1] \rho(\mathbf{r}). \end{aligned} \quad (18)$$

We determine the induced charge profile numerically by discretizing Eq. (18) of the ICC method and solving for  $h(\mathbf{r})$ . We focus on the case of sharp dielectric boundaries although the equation and method are valid for any  $\epsilon(\mathbf{r})$ . To our knowledge, Eq. (18) has not been previously derived for this general case.

### C. Point charges

When the source charges (SC) are point charges at discrete locations, the source charge density is given by

$$\rho(\mathbf{r}) = \sum_k z_k e \delta(\mathbf{r}-\mathbf{r}_k), \quad (19)$$

where source charge  $k$  with valence  $z_k$  is located at  $\mathbf{r}_k$  and  $e$  is the elementary charge. Because they are point charges, the induced charge around each charge  $k$  has a density [44]

$$-z_k e \frac{\epsilon(\mathbf{r}_k) - 1}{\epsilon(\mathbf{r}_k)} \delta(\mathbf{r}-\mathbf{r}_k), \quad (20)$$

if the dielectric is locally uniform around the source charge. Therefore, the contribution to  $h$  from the induced charge around the source charges is

$$h_{SC}(\mathbf{r}) = - \sum_k z_k e \frac{\epsilon(\mathbf{r}_k) - 1}{\epsilon(\mathbf{r}_k) \epsilon_0} \delta(\mathbf{r}-\mathbf{r}_k). \quad (21)$$

Substituting this into Eq. (18) gives

$$\begin{aligned} h(\mathbf{r}) \epsilon(\mathbf{r}) - \int_{\mathcal{D}} h(\mathbf{r}') \nabla_{\mathbf{r}'} \epsilon(\mathbf{r}') \cdot \nabla_{\mathbf{r}'} G(\mathbf{r}-\mathbf{r}') d\mathbf{r}' \\ = \nabla_{\mathbf{r}} \epsilon(\mathbf{r}) \cdot \nabla_{\mathbf{r}} \psi_e(\mathbf{r}), \end{aligned} \quad (22)$$

where

$$\nabla^2 \psi_e(\mathbf{r}) = - \frac{e}{\epsilon_0} \sum_k \frac{z_k}{\epsilon(\mathbf{r}_k)} \delta(\mathbf{r}-\mathbf{r}_k) \quad (23)$$

and  $h$  refers solely to the induced charges *other* than those around the source charges. Equation (23) gives the electrostatic potential resulting from the source charges at point  $\mathbf{r}$ , namely

$$\psi_e(\mathbf{r}) = \frac{e}{4\pi\epsilon_0} \sum_k \frac{z_k}{\epsilon(\mathbf{r}_k) |\mathbf{r}-\mathbf{r}_k|}. \quad (24)$$

It is important to note that if the source charge were an ion represented, for example, as a point charge at the center of a hard dielectric sphere with a dielectric coefficient different from that of the surrounding medium, then the induced

charge on the ion surface must also be determined [41,42]; this induced charge would give another contribution to  $h(\mathbf{r})$  on the LHS of Eq. (14). Since, in a computer simulation, the source charges are moving, the geometry of the dielectric pattern would constantly change, increasing computation time substantially. For this reason, we assign the interior of the ion the same dielectric coefficient as the surrounding medium.

#### D. Sharp dielectric boundaries

Next, we turn to the special case of sharp dielectric boundaries in which the dielectric coefficient jumps from one value to another across the boundary surface. Then the induced charge is a surface charge on the dielectric interfaces (if the induced charge around the source charges is not considered), and the integrals in Eq. (18) become surface integrals over the dielectric interface  $\mathcal{B}$  [29]:

$$\begin{aligned} h(\mathbf{s})\varepsilon(\mathbf{s}) - \Delta\varepsilon(\mathbf{s}) \int_{\mathcal{B}} h(\mathbf{s}') \nabla_{\mathbf{s}} G(\mathbf{s} - \mathbf{s}') \cdot \mathbf{n}(\mathbf{s}) d\mathbf{s}' \\ = \Delta\varepsilon(\mathbf{s}) \nabla \psi_e(\mathbf{s}) \cdot \mathbf{n}(\mathbf{s}). \end{aligned} \quad (25)$$

The dielectric coefficient on the boundary  $\varepsilon(\mathbf{s})$  is defined to be the arithmetic mean of the two dielectric coefficients on each side of the boundary, and the dielectric jump  $\Delta\varepsilon(\mathbf{s})$  is the difference of the two dielectric coefficients [in the direction of the local unit normal of the surface  $\mathbf{n}(\mathbf{s})$ ].

To solve Eq. (25) numerically, the surface  $\mathcal{B}$  must be discretized; specifically, each discrete surface element  $\beta$  of  $\mathcal{B}$  is characterized by its center of mass  $\mathbf{s}_\beta$ , area  $a_\beta$ , unit normal  $\mathbf{n}_\beta$ , value of the mean dielectric coefficient  $\varepsilon_\beta$ , and value of the dielectric jump  $\Delta\varepsilon_\beta$ . Both the potential  $\psi_e$  [Eq. (24)] and the Green's function (of  $\mathbb{R}^3$ )  $G$  are known functions. The integrals in Eq. (25) are then discretized as sums over the surface elements  $\beta$ ,

$$\sum_{\beta} h_{\beta} \left( \delta_{\alpha\beta} \varepsilon_{\beta} - \Delta\varepsilon_{\alpha} \frac{\partial G_{\alpha\beta}}{\partial n_{\alpha}} a_{\beta} \right) = \Delta\varepsilon_{\alpha} \frac{\partial \psi_{\alpha}}{\partial n_{\alpha}} \quad (26)$$

for a given  $\alpha$ , where  $\delta_{\alpha\beta}$  is the Kronecker  $\delta$ ,

$$\frac{\partial G_{\gamma\beta}}{\partial n_{\gamma}} = \begin{cases} \nabla_{\mathbf{s}_{\gamma}} G(\mathbf{s}_{\gamma} - \mathbf{s}_{\beta}) \cdot \mathbf{n}_{\gamma} & \text{for } \beta \neq \gamma \\ 0 & \text{for } \beta = \gamma \end{cases} \quad (27)$$

and

$$\frac{\partial \psi_{\beta}}{\partial n_{\beta}} = \nabla \psi_e(\mathbf{s}_{\beta}) \cdot \mathbf{n}_{\beta}. \quad (28)$$

This can be rewritten in matrix form as

$$\mathbf{A}\mathbf{h} = \mathbf{c}, \quad (29)$$

where each element of the matrix  $A$  is given by

$$A_{\alpha\beta} = \delta_{\alpha\beta} \varepsilon_{\beta} - \Delta\varepsilon_{\alpha} \frac{\partial G_{\alpha\beta}}{\partial n_{\alpha}} a_{\beta}. \quad (30)$$

Each element of the column vector  $\mathbf{h}$  is given by  $h_{\beta}$  and each element of the column vector  $\mathbf{c}$  is given by

$$c_{\alpha} = \Delta\varepsilon_{\alpha} \frac{\partial \psi_{\alpha}}{\partial n_{\alpha}}. \quad (31)$$

This is the same matrix formulation introduced by Hoshi *et al.* [41], although our derivation and resulting formulas are more general. The discretization of the more general Eq. (18) is similar and also produces a linear matrix equation.

In simulations of point charges, the source charges contribute only the RHS of Eq. (29); the matrix  $A$  is given only by dielectric profile and the Green's function. Thus, the inverse of  $A$  (or any factorization of  $A$ ) need only be computed *once* for a given geometry and dielectric profile. The computational burden is then reduced to approximately  $N^2$  operations compared to the  $N^3$  that would be needed if the matrix had to be inverted at each simulation step (where  $N$  is the number of surface elements). Another useful method is GMRES [45,46] which solves the matrix equation for  $\mathbf{h}$  once with  $O(N^2)$  operations. While GMRES is significantly slower than backsubstitution after LU factorization (which we use here), it is useful in cases when the dielectric boundaries move between MC steps (such as when the charge is surrounded by a dielectric sphere that moves along with the charge); in such a situation, LU factorization would require  $N^3$  operations for every MC step. In the context of ASC solvation methods, Pomelli and Tomasi [42,43] have also developed a fast iterative algorithm.

### III. SIMULATIONS

This paper presents the ICC method and tests its usefulness in MC simulations. The algorithm is equally applicable to Brownian dynamics (BD) and MD simulations. In this paper, we use the canonical ensemble; thus, the volume of the system, the numbers of particles of the various species, and the temperature  $T$  are the fixed and independent parameters of the ensemble. The MC techniques we use are standard and the reader is referred to Refs. [1–3] for further details. In this section, we describe the calculation of the electrostatic energy of a system and various tools to accelerate this calculation.

#### A. Calculation of the energy

In a MC simulation, the change in the energy of the system determines acceptance or rejection of a MC step. The probability of accepting a trial move in the canonical ensemble is  $\min[1, \exp(-\Delta W/kT)]$ , where  $k$  is Boltzmann's constant and  $\Delta W$  is the energy change of the move, the quantity we need to calculate.

The electrostatic potential at any point  $\mathbf{r}$  in the system is given by

$$\psi(\mathbf{r}) = \frac{e}{4\pi\varepsilon_0} \sum_i \frac{z_i}{\varepsilon_i |\mathbf{r} - \mathbf{r}_i|} + \frac{1}{4\pi} \sum_{\alpha} \frac{h_{\alpha} a_{\alpha}}{|\mathbf{r} - \mathbf{s}_{\alpha}|}, \quad (32)$$

where the indices  $i$  and  $\alpha$  range over the source point charges and the dielectric surface elements, respectively, and  $\varepsilon_i$  is the

dielectric coefficient of the region where the  $i$ th charge resides. The electrostatic energy of the system is determined from the potential energy of the source charges:

$$W = \frac{e}{2} \sum_j z_j \psi(\mathbf{r}_j). \quad (33)$$

The terms  $i=j$  should be omitted from the double sum that Eqs. (32) and (33) form together.

In MC simulations that involve pairwise additive intermolecular potentials, the energy change of the system is equal to the energy change of the one moved particle, making the computational burden of calculating  $\Delta W$  of order of the number of particles. In a system with dielectric boundaries, moving one charged particle changes the charge induced on all dielectric boundaries, which, in turn, changes the electrostatic potential for *all* charged particles. In this kind of system, moving one particle requires recomputing the interaction energies of the moved particle with all the other particles, as in a simulation without dielectric boundaries. In addition, a particle move also requires recomputing the interaction energies between all the induced charges and all charged particles. For this calculation, the linearity of the matrix, Eq. (29), produces significant computational savings. Every element  $c_\alpha$  of the vector  $\mathbf{c}$  is a sum of the normal components of the electric fields produced by the source charges. Since most of the charges do not move in a MC step, their contribution to  $c_\alpha$  does not have to be computed. If  $\Delta \mathbf{c}$  is the change of  $\mathbf{c}$  that contains only the contributions from the moved charge, then the change in the induced charges is

$$\Delta \mathbf{h} = \mathbf{A}^{-1} \Delta \mathbf{c}, \quad (34)$$

where  $\mathbf{A}^{-1}$  is the inverse of matrix  $\mathbf{A}$ . The induced charge after a simulation step (denoted by superscript *new*) is calculated from the induced charge before the simulation step (denoted by superscript *old*) as  $\mathbf{h}^{new} = \mathbf{h}^{old} + \Delta \mathbf{h}$ . The energy change due to the polarization charges induced by the displacement of the  $i$ th charge is

$$\begin{aligned} \Delta W_{ind} = & \frac{z_i e}{8\pi} \sum_\alpha a_\alpha \left( \frac{h_\alpha^{new}}{|\mathbf{r}_i^{new} - \mathbf{s}_\alpha|} - \frac{h_\alpha^{old}}{|\mathbf{r}_i^{old} - \mathbf{s}_\alpha|} \right) \\ & + \frac{e}{8\pi} \sum_{j \neq i} \sum_\alpha z_j \frac{a_\alpha \Delta h_\alpha}{|\mathbf{r}_j - \mathbf{s}_\alpha|}. \end{aligned} \quad (35)$$

Only the distances  $|\mathbf{r}_i^{new} - \mathbf{s}_\alpha|$  need to be calculated in a MC step; all other distances have been previously calculated and can be stored in an array. This precalculation greatly reduces computation time because a rate-limiting step in the MC simulation is the computation of the square root when calculating vector lengths.

The energy calculations we discuss are valid only for movements of a charge *within* a dielectric. If a charge moves across a dielectric boundary, the interaction energy between the charge and its surrounding dielectric must be included in the energy calculation.

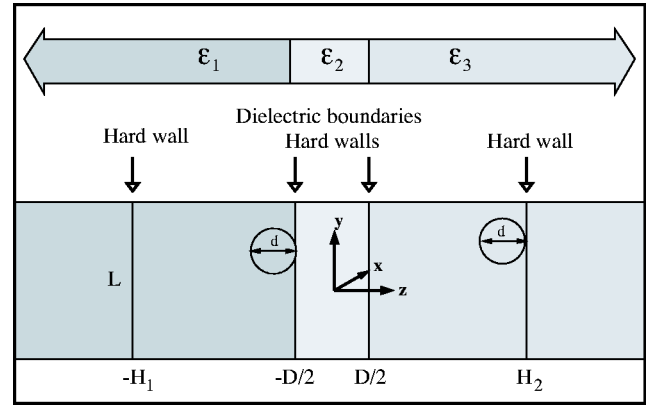


FIG. 1. The geometry of the simulation cell with two planar boundaries. Periodic boundary conditions are applied in the  $x$  and  $y$  directions. The simulation cell is closed by hard walls at  $z = -H_1$  and  $z = H_2$ . These walls are not dielectric boundaries; the dielectric remains uniform going through these walls:  $\epsilon = \epsilon_1$  and  $\epsilon = \epsilon_3$  for  $z < -H_1$  and  $z > H_2$ , respectively. The ions are restricted to their host dielectric domain by making the dielectric boundaries at  $z = -D/2$  and  $z = D/2$  hard walls. The simulation cell for the simpler case has only one dielectric boundary at  $z = 0$  with dielectric domains  $\epsilon_1$  and  $\epsilon_2$ .

## B. Periodic boundary conditions

In this paper, we test the ICC method in two specific geometries. In the first geometry, two dielectric media with dielectric coefficients  $\epsilon_1$  and  $\epsilon_2$  are separated by an impenetrable, planar surface. Here an analytic solution exists (derived via the electrostatic image charge method [44]) that is efficiently incorporated into computer simulations [5,47]. The other case (Fig. 1) has three dielectrics separated by two parallel, impenetrable, planar dielectric interfaces. Both systems are homogeneous in the  $x$  and  $y$  directions, but inhomogeneous in the  $z$  direction.

The finite (computational) system is expanded in the  $x$  and  $y$  directions by applying periodic boundary conditions (PBCs) with periodic replicas of the simulation cell in the given direction. Both the source charges and the induced charges have periodic replicas. When a particle is moved out of the central simulation cell, its corresponding periodic replica enters from the opposite side [1–3]. To determine a distance between two charges (or between a charge and the center of a surface element), we choose the closest replica to the given charge. This implementation of PBCs follows the “minimum image convention” [1–3]. (Note the distinction between the use of the word image here and in the electrostatic image charge method.)

## C. Simulation method and the model

The simulation cell is shown in Fig. 1. The cell dimension is  $L$  in both the  $x$  and  $y$  directions and  $H_1 + H_2$  in the  $z$  direction. These values must be large enough to avoid numerical artifacts resulting from the periodicity, cutoff potentials, and finite size of the simulation cell. Beyond the hard walls confining the ions in the  $z$  direction, the dielectric continues without any change in  $\epsilon$ , but this region is not accessible to the ions. The simulation cell is overall electroneutral.

TABLE I. Some details of the ICC simulations.  $N$  is the number of surface elements.  $N_+^{\text{left}}$ ,  $N_-^{\text{left}}$ ,  $N_+^{\text{right}}$ , and  $N_-^{\text{right}}$  are the number of positive and negative ions on the left or right sides.  $N_{\text{MC}}$  is the number of MC steps. An attempt to move up to  $N_{\text{ions}}$  is made in one MC step, where  $N_{\text{ions}}$  is the total number of ions in the simulation cell. The “speed” is measured in  $N_{\text{MC}}/(\text{min CPU})$ , the number of MC steps performed in 1 min on 1 processor (in real time, using 2.4 GHz Pentium Xenon processors of a Linux cluster). For comparison, the speed is about  $2800 N_{\text{MC}}/(\text{min CPU})$  for an image charge simulation.  $N_{\text{CPU}}$  is the number of processors used. “Fig.” denotes the figure in which results are shown for the given simulation. Results for simulations (2) and (5) are not shown in the figures because they are indistinguishable from the results of simulations (1) and (4), respectively.  $L$  and  $H_2$  are the dimensions of the simulation cell in  $x$ - $y$  and  $z$  directions, respectively. In simulations (8)–(15),  $H_1 = H_2$ .

| No. | Geometry | $L/d$ | $H_2/d$ | $\Delta x/d$ | $N$  | $N_+^{\text{left}}$ | $N_-^{\text{left}}$ | $N_+^{\text{right}}$ | $N_-^{\text{right}}$ | $N_{\text{MC}}/10^3$ | Speed | $N_{\text{CPU}}$ | Fig. |
|-----|----------|-------|---------|--------------|------|---------------------|---------------------|----------------------|----------------------|----------------------|-------|------------------|------|
| 1   | 2 80     | 20    | 31.22   | 1/2          | 1600 |                     |                     | 100                  | 100                  | 6400                 | 37.5  | 40               | 4(c) |
| 2   | 2 80     | 20    | 31.22   | 5/6          | 576  |                     |                     | 100                  | 100                  | 6000                 | 104.7 | 30               |      |
| 3   | 2 80     | 21    | 31.22   | 7/6          | 289  |                     |                     | 100                  | 100                  | 3200                 | 210.5 | 16               | 4(c) |
| 4   | 80 40    | 20    | 31.13   | 1/2          | 1600 |                     |                     | 100                  | 100                  | 2000                 | 36.9  | 10               | 5(b) |
| 5   | 80 40    | 20    | 31.13   | 5/6          | 576  |                     |                     | 100                  | 100                  | 2000                 | 89.1  | 10               |      |
| 6   | 80 40    | 21    | 31.13   | 7/6          | 289  |                     |                     | 100                  | 100                  | 2000                 | 163.5 | 10               | 5(b) |
| 7   | 80 40    | 21    | 31.13   | 3/2          | 169  |                     |                     | 100                  | 100                  | 3000                 | 555.1 | 10               | 5(b) |
| 8   | 80 40    | 20    | 19.87   | 1/2          | 1600 | 60                  | 60                  | 60                   | 60                   | 1925                 | 27.1  | 10               | 6(a) |
| 9   | 80 40    | 20    | 19.87   | 1/2          | 1600 | 60                  | 61                  | 61                   | 60                   | 1935                 | 27.7  | 10               | 6(b) |
| 10  | 80 20 80 | 20    | 21.18   | 2/3          | 1800 | 60                  | 60                  | 60                   | 60                   | 663                  | 1.8   | 50               | 7(a) |
| 11  | 80 20 80 | 20    | 21.18   | 1            | 800  | 60                  | 60                  | 60                   | 60                   | 1297                 | 9.6   | 40               | 7(a) |
| 12  | 80 20 80 | 20    | 21.18   | 4/3          | 450  | 60                  | 60                  | 60                   | 60                   | 4990                 | 30.3  | 40               | 7(a) |
| 13  | 40 80 40 | 20    | 21.18   | 2/3          | 1800 | 60                  | 60                  | 60                   | 60                   | 1023                 | 1.8   | 50               | 7(b) |
| 14  | 40 80 40 | 20    | 21.18   | 1            | 800  | 60                  | 60                  | 60                   | 60                   | 2200                 | 10.4  | 30               | 7(b) |
| 15  | 40 80 40 | 20    | 21.18   | 4/3          | 450  | 60                  | 60                  | 60                   | 60                   | 3152                 | 31.2  | 20               | 7(b) |

In some cases we choose the number of cations and anions to be different in the various dielectric domains, resulting in electrical double layers at the dielectric boundaries.

The ions are represented as charged, hard spheres [5]. Nevertheless, because the ions are in different dielectrics, it is necessary to be more precise. The ions are represented as point charges embedded at the center of hard, dielectric spheres of diameter  $d$  with the same dielectric coefficient as that of the medium surrounding them. The ions cannot leave their host dielectric because the dielectric boundaries act as hard walls. The charge of the cations and the anions is  $+e$  and  $-e$ , respectively, and all ion species are given the same diameter.

The targeted bulk cation and anion concentration is  $\rho_0 = 0.5 \text{ mole/dm}^3$ . This concentration corresponds to a reduced density  $\rho_{\text{ions}}^* = N_{\text{ions}} d^3 / V = 0.0163$ , where  $N_{\text{ions}}$  is the total number of ions, in the particular case of  $d = 3 \text{ \AA}$ . This is a low density system because the water is modeled as a continuum dielectric. The density profiles computed in our simulations depend only on  $z$  and are given normalized to the bulk density:  $\rho(z)/\rho_0$ . Acceptable statistical variations of density profiles  $\rho(z)$  in such low-density systems requires long simulations or, alternately, many simulations with different random initial configurations run simultaneously on separate processors and then averaged. Table I lists computational details of the ICC simulations.

The strength of the ionic interactions can be described by the dimensionless coupling tensor

$$q_{ij}^* = \frac{z_i z_j e^2}{4 \pi \epsilon \epsilon_0 k T d}, \quad (36)$$

where  $k$  is Boltzmann’s constant. If the ions had different diameters, these would be incorporated into the definition of  $q_{ij}^*$ . Each element in the tensor corresponds to the interaction energy between two ions in contact, measured in  $kT$ . For a symmetric electrolyte the coupling is described by a scalar. This coupling constant shows how a given interaction strength can be achieved by different dielectric coefficients, temperatures, and ion sizes.

In our simulations,  $q^* = 2.321$  and  $q^* = 4.642$ , corresponding to monovalent ions with  $d = 3 \text{ \AA}$  at  $T = 300 \text{ K}$  in dielectric media with  $\epsilon = 80$  and  $\epsilon = 40$ , respectively. However, our conclusions are not tied to any particular value of  $d$  and coupling constant. Using the coupling constant makes a more general treatment of other parameters possible. Scaling lengths and distances by  $d$  while keeping the coupling constant unchanged means that the same values of  $\Delta x$  and  $L$ , in units of  $d$ , can be used. Note that because the dielectric coefficient has a strong spatial variation in some systems, ionic coupling might change with location. One must construct the grid and choose the cell dimensions in such geometries with extra care.

## IV. RESULTS AND DISCUSSION

### A. One dielectric boundary plane

We first present MC results for one sharp planar boundary with ions present on only one side (on the right, subscripted by 2). We use this somewhat overstudied system for the same reason it is overstudied: a simple, analytical solution is available with the electrostatic image charge method [44]. Applying this method in a MC simulation is straightforward [47]

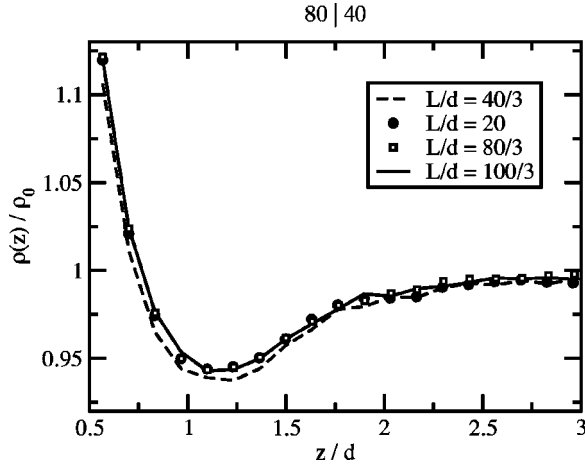


FIG. 2. The normalized density profiles calculated with the image charge method of an electrolyte in an  $\epsilon_2=40$  dielectric near a boundary with an  $\epsilon_1=80$  dielectric. The various curves refer to various cell widths  $L/d=40/3$ ,  $60/3$ ,  $80/3$ , and  $100/3$ . For all subsequent MC simulations,  $L\approx 20d$  is chosen so that  $L/\Delta x$  is an integer.

and results in a relatively fast code with which we can quantify errors introduced by the ICC method. Analytic solutions are available for other geometries (for example, a dielectric sphere [44]), but these are generally series of special functions that require many terms to calculate accurately for ions near the interface. This would result in relatively slow MC simulations compared to the one-plane case computed with image charges.

For the case of a single dielectric boundary we report two simulations: (a)  $\epsilon_1=2$  and  $\epsilon_2=80$  and (b)  $\epsilon_1=80$  and  $\epsilon_2=40$ . Case (a) represents a large dielectric jump that is encountered in biological applications. Because  $\epsilon_1 < \epsilon_2$ , the ions are repelled by the induced charge. Case (b) is the opposite and so ions are attracted to the boundary. We choose  $\epsilon_2=40$  because significantly smaller values are not physically realistic; ions cannot be dissolved in low-dielectric solvents.

The ICC method uses several geometric parameters as inputs, specifically  $H_1$ ,  $H_2$ ,  $L$ , and  $\Delta x$  given in terms of our length scale  $d$ , the ion diameter. Previous MC simulations show that  $H_1/d=H_2/d\gtrsim 20$  is sufficiently large for the ion reservoirs [48–51]. Figure 2 shows the density profiles for the  $\epsilon_1=80|\epsilon_2=40$  case with various cell widths  $L$  calculated using image charges. For the values of the coupling constant and density we use, above  $L/d\approx 20$  the profiles are indistinguishable. In all subsequent simulations we use this value.

Unlike the system dimensions  $H_1$ ,  $H_2$ , and  $L$ , the parameter  $\Delta x$  directly influences the accuracy of the computed ion/dielectric interface interaction. Because  $\Delta x$  represents the discretization of the actually continuous surface charge distribution, the proper choice of  $\Delta x$  depends on the system being studied. In addition, curved interfaces require some curvature correction on each surface element [41,52]. In the ICC method, these corrections change only the fill time of the matrix  $A$ , and not the size of the matrix. Since the matrix

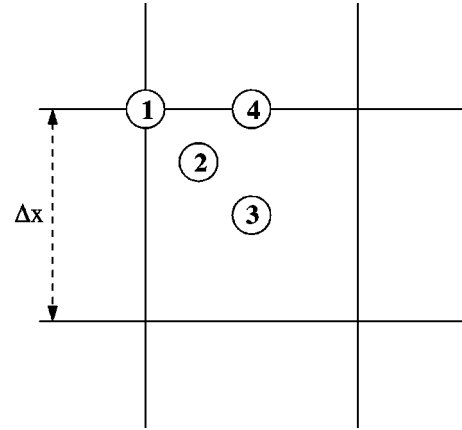


FIG. 3. The figure locates four points on one dielectric surface element of the computational grid. To analyze errors due to the discretization of the dielectric interface, a test charge is located above one of these four locations (out of the plane) at a distance  $z$  from the plane.

is computed only once for a particle simulation, increased fill time has little effect on simulation time.

For the planar dielectric interface, we explore the effect of  $\Delta x$  by considering the energy of a single point charge  $e$  in the vicinity of the dielectric boundary. This is the energy due to the polarization of the boundary by the point charge, corresponding to the interaction energy between the point charge at  $\mathbf{r}_i$  and the induced charges, namely

$$W_{pol}^i = \frac{e}{8\pi} \sum_{\alpha} \frac{h_{\alpha} a_{\alpha}}{|\mathbf{r}_i - \mathbf{s}_{\alpha}|}. \quad (37)$$

Figure 3 defines the  $x$ - $y$  coordinates of four charges located above a dielectric surface element at  $\mathbf{r}_1$ ,  $\mathbf{r}_2$ ,  $\mathbf{r}_3$ , and  $\mathbf{r}_4$ . In the discretization of the dielectric interface, the induced surface charge is a point charge in the center of the surface element. Position 3 is above the discretized induced charge, while position 1 is above a corner (farthest from the induced charge). With a source charge at one of these locations  $\mathbf{r}_i$  at a distance  $z$  from the interface, the polarization energy  $W_{pol}^i$  is computed as a function of  $z$ . Figure 4(a) compares the ICC result for each source charge position to the analytic result for the ideal dielectric boundary separating  $\epsilon_1=2$  and  $\epsilon_2=80$ . Results for  $z/d < 1/2$  are not shown, because the centers and charges of hard-sphere ions are excluded from that region. The width of the surface element is  $\Delta x/d=5/6$ . The ideally infinite dielectric planar interface used for the image charge calculation is given a finite length of  $L/d=20$ , the same cell width used in all MC simulations. PBCs are not used in these ICC calculations; they are used only in the MC simulations.

The polarization energy is sensitive to position when the test charge is close to the discretized boundary in the simulation. The deviations from the exact result are relatively large when the test charge is in position 3 (closest to the discretized induced charge) and when it is in position 1 (farthest from the discretized induced charge) with opposite signs. This is because the induced surface charge that is ideally spread on the surface element is represented as a point

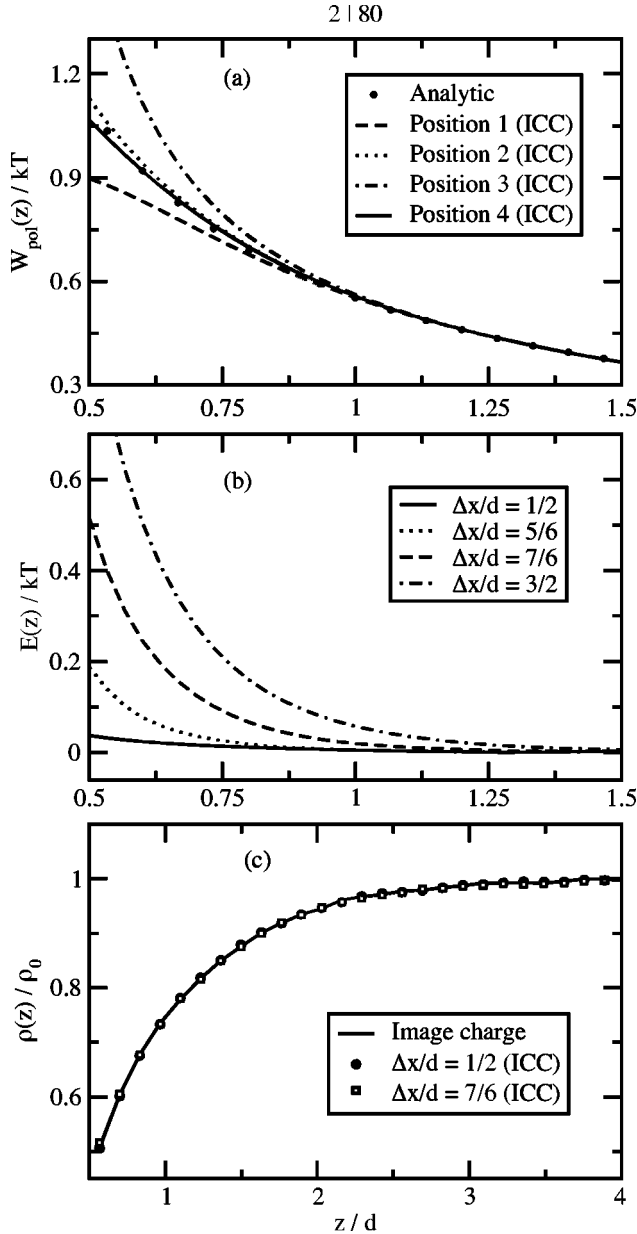


FIG. 4. (a) The polarization energy of a point charge of magnitude  $e$  as a function of distance  $z$  from a flat dielectric boundary for  $\epsilon_1=2$  and  $\epsilon_2=80$ . The test charge is in one of the four positions above the grid as shown in Fig. 3. The width of a surface element square is  $\Delta x/d=5/6$ . (b) The error  $E(z)$  defined in Eq. (38) for all four charge positions for  $\Delta x/d=1/2, 5/6, 7/6$ , and  $3/2$ . Note that  $E(z) \rightarrow 0$  as  $\Delta x/d \rightarrow 0$  and that, for numerical purposes,  $\Delta x/d = 1/2$  gives sufficiently small errors. (c) Normalized density profiles from ICC-MC simulations with  $\Delta x/d=1/2$  and  $7/6$  compared with MC simulations using image charges. The profiles computed using  $\Delta x/d=5/6$  were indistinguishable from the profiles computed using  $\Delta x/d=1/2$ .

charge in the center of the square. Thus, the interaction with the induced charge is overestimated when the test charge is close to the center.

Since the polarization energy (37) is an important component of the system energy (35), the errors shown in Fig. 4(a) (for a given  $\Delta x$ ) must be so small that they do not affect the

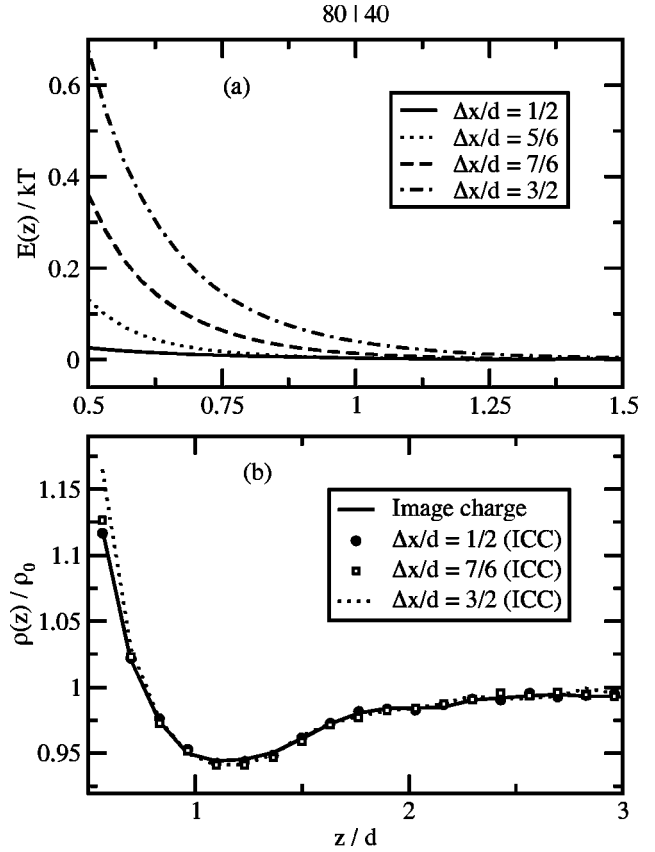


FIG. 5. (a) The error  $E(z)$  defined in Eq. (38) for a flat dielectric boundary with  $\epsilon_1=80$  and  $\epsilon_2=40$  for the four charge positions shown in Fig. 3 with  $\Delta x/d=1/2, 5/6, 7/6$ , and  $3/2$ . As in Fig. 4,  $E(z) \rightarrow 0$  as  $\Delta x/d \rightarrow 0$ . (b) Normalized density profiles from ICC-MC simulations with  $\Delta x/d=1/2, 7/6$ , and  $3/2$  compared with MC simulations using image charges. The profiles computed using  $\Delta x/d=5/6$  were indistinguishable from the profiles computed using  $\Delta x/d=1/2$ .

density profiles. To show that these errors can be controlled by choosing  $\Delta x$  small enough, we consider the error index

$$E(z) = \frac{1}{4} \sum_{i=1}^4 |W_{pol}^i(z) - W_{IC}(z)|, \quad (38)$$

where  $W_{IC}(z)$  is the analytic polarization energy calculated from the image charge method [44] and the four charge positions  $\mathbf{r}_i$  (with varying  $z$ ) are those shown in Fig. 3. Figure 4(b) shows that  $E(z) \rightarrow 0$  as  $\Delta x \rightarrow 0$ . For numerical purposes, we find that  $\Delta x/d = 1/2$  sufficiently reduces the error. Figure 4(c) shows that computed ion density profiles for the  $\epsilon_1 = 2 | \epsilon_2 = 80$  case with various  $\Delta x$  agree well with MC simulations using the image charge method rather than the ICC method. We find that even for  $\Delta x$ 's where  $E(z)$  is not 0, the ICC-MC density profiles are indistinguishable and agree with MC simulations using the image charge method.

We examine the  $\epsilon_1=80 | \epsilon_2=40$  case in a similar way. Figure 5(a) shows  $E(z)$  for various  $\Delta x$  and Fig. 5(b) shows the results of several MC simulations, each using a different  $\Delta x$ . The conclusions about errors are similar to those of the  $\epsilon_1=2 | \epsilon_2=80$  case.

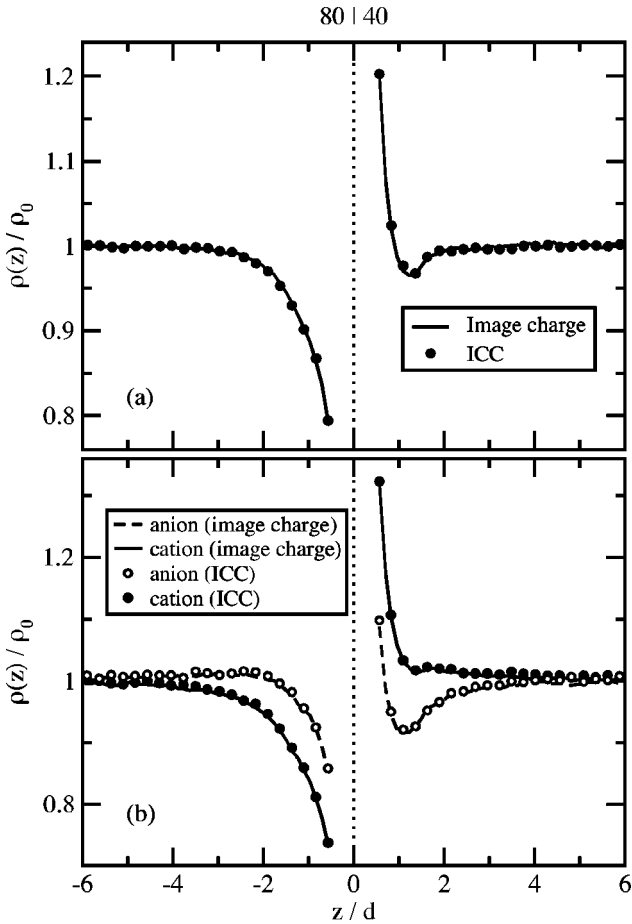


FIG. 6. The normalized density profiles of electrolytes in a system of two dielectrics with coefficients  $\epsilon_1=80$  and  $\epsilon_2=40$  separated by a flat boundary at  $z=0$ . ICC-MC results are compared with MC results using image charges. The number of cations and anions on the two sides of the dielectric boundary is (a) equal and (b) different. In case (b), double layers are formed near the interface and separate profiles for the cations and anions are shown. In case (a), cation and anion profiles are the same (apart from statistical noise). The width of a dielectric surface element is  $\Delta x/d=1/2$ .

Next, we consider a case in which ions are present on both sides of  $\epsilon_1=80|\epsilon_2=40$  interface. Figure 6(a) shows the density profiles with an electroneutral electrolyte on each side of the interface. In this and the other simulations presented so far, the cation profiles coincide with the anion profiles (apart from statistical noise). In Fig. 6(b), we show density profiles calculated when the number of cations and anions is not equal on each side (Table I). The extra charges are attracted to the regions near the dielectric interface and form electrical double layers there. The agreement between image charge and the ICC results (with  $\Delta x/d=1/2$ ) is good for both anion and cation densities.

**B. Two dielectric boundary planes**

Next we consider a dielectric slab with dielectric coefficient  $\epsilon_2$  embedded between two semiinfinite dielectrics of

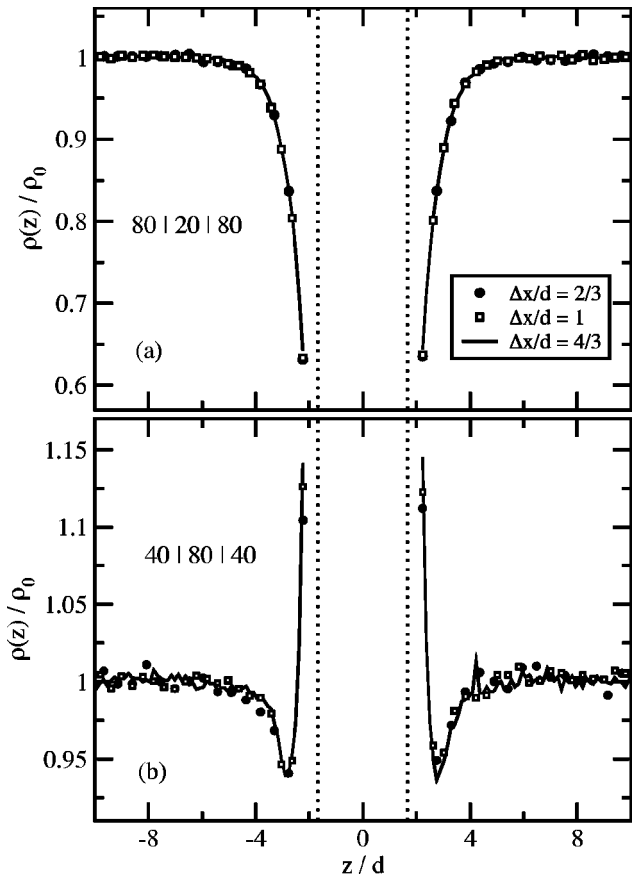


FIG. 7. The normalized density profiles of electrolytes outside a dielectric slab of width  $D/d=10/3$  calculated from the ICC method. The dielectric coefficient of the slab and the outside regions are (a)  $\epsilon_2=20$  and  $\epsilon_1=\epsilon_3=80$ , respectively, and (b)  $\epsilon_2=80$  and  $\epsilon_1=\epsilon_3=40$ , respectively. The widths of a surface element are  $\Delta x/d=2/3, 1, \text{ or } 4/3$ .

dielectric coefficients  $\epsilon_1$  and  $\epsilon_3$  (Fig. 1). We use  $\epsilon_1=\epsilon_3$ . In Fig. 7, ICC-MC results are shown using different  $\Delta x$  for a slab of width  $D/d=10/3$  with (a)  $\epsilon_1=80|\epsilon_2=20|\epsilon_3=80$  and (b)  $\epsilon_1=40|\epsilon_2=80|\epsilon_3=40$ . In each case, the computed density profiles converge as  $\Delta x$  decreases. The profiles are very similar to those obtained for the single boundary case that corresponds to a semiinfinite slab geometry. Apparently the density profiles are governed by the interaction of the ions with the closest dielectric boundary.

This two-interface geometry provides an additional test of the ICC method because the matrix  $A$  is not diagonal; with two interfaces, induced charges on one plane induce (further) charges on the other plane and therefore  $\partial G_{\alpha\beta}/\partial n_\alpha \neq 0$  for all  $\alpha$  and  $\beta$  in Eq. (26). The number of operations in the matrix multiplication  $A^{-1}\mathbf{c}$  is now of order  $N^2$  instead of  $N$ . The simulations are slower, but still practical. Simulations (1)–(7) (Table I) show that the speed of computation is roughly proportional to the inverse number of surface elements  $N$  in systems with one interface. If the matrix  $A$  is not diagonal [simulations (10)–(15)] this relation is nonlinear; it is proportional to  $1/N^2$ . Nevertheless, using a cluster of computers, as described earlier, makes such calculations feasible.

## V. CONCLUSION

We report a different solution of the extremum condition of the functional introduced by Allen *et al.* [29]. After discretization, this solution produces a matrix equation convenient for molecular simulations.

## ACKNOWLEDGMENTS

The authors wish to thank David Busath for his many discussions. The authors are also grateful for the use of the facilities of the Ira & Marylou Fulton Supercomputer Center of Brigham Young University.

- 
- [1] M.P. Allen and D.J. Tildesley, *Computer Simulation of Liquids* (Oxford, New York, 1987).
- [2] D. Frenkel and B. Smit, *Understanding Molecular Simulations* (Academic Press, San Diego, 1996).
- [3] R.J. Sadus, *Molecular Simulation of Fluids: Theory, Algorithms, and Object-orientation* (Elsevier, Amsterdam, 1999).
- [4] T. Schlick, *Molecular Modeling and Simulation* (Springer-Verlag, New York, 2002).
- [5] G.M. Torrie, J.P. Valleau, and G.N. Patey, *J. Chem. Phys.* **76**, 4615 (1982).
- [6] J.S. Newman, *Electrochemical Systems* (Prentice-Hall, Englewood Cliffs, NJ, 1991).
- [7] W. Schmickler, *Interfacial Electrochemistry* (Oxford University Press, New York, 1996).
- [8] C. Jacoboni and P. Luigi, *The Monte Carlo Method for Semiconductor Device Simulation* (Springer-Verlag, New York, 1989).
- [9] B. Honig and A. Nichols, *Science* **268**, 1144 (1995).
- [10] J. Tomasi and M. Persico, *Chem. Rev. (Washington, D.C.)* **94**, 2027 (1994).
- [11] V.A. Parsegian, *Nature (London)* **221**, 844 (1969).
- [12] B. Neumcke and P. Lauger, *Biophys. J.* **9**, 1160 (1969).
- [13] D.P. Tieleman, P.C. Biggin, G.R. Smith, and M.S.P. Sansom, *Q. Rev. Biophys.* **34**, 473 (2001).
- [14] D.G. Levitt, *Biophys. J.* **22**, 209 (1978); **22**, 221 (1978).
- [15] P.C. Jordan, *Biophys. Chem.* **13**, 203 (1981); *Biophys. J.* **39**, 157 (1982); **41**, 189 (1983).
- [16] S.-H. Chung, M. Hoyles, T. Allen, and S. Kuyucak, *Biophys. J.* **75**, 793 (1998).
- [17] S.-H. Chung, T. Allen, M. Hoyles, and S. Kuyucak, *Biophys. J.* **77**, 2517 (1999).
- [18] B. Corry, T. Allen, S. Kuyucak, and S.-H. Chung, *Biophys. J.* **80**, 195 (2001).
- [19] M. Hoyles, S. Kuyucak, and S.-H. Chung, *Phys. Rev. E* **58**, 3654 (1998).
- [20] G. Moy, B. Corry, S. Kuyucak, and S.-H. Chung, *Biophys. J.* **78**, 2349 (2000).
- [21] B. Corry, S. Kuyucak, and S.-H. Chung, *Biophys. J.* **78**, 2364 (2000).
- [22] P. Graf, A. Nitzan, M. Kurnikova, and R. Coalson, *J. Phys. Chem. B* **101**, 5239 (1997).
- [23] W. Im and B. Roux, *J. Chem. Phys.* **115**, 4850 (2001).
- [24] W. Nonner, L. Catacuzzeno, and B. Eisenberg, *Biophys. J.* **79**, 1976 (2000).
- [25] W. Nonner, D. Gillespie, D. Henderson, and B. Eisenberg, *J. Phys. Chem. B* **105**, 6427 (2001).
- [26] Z. Schuss, B. Nadler, and R.S. Eisenberg, *Phys. Rev. E* **64**, 036116 (2001).
- [27] B. Nadler, U. Hollerbach, and R.S. Eisenberg, *Phys. Rev. E* **68**, 021905 (2003).
- [28] T. Bastug and S. Kuyucak, *Biophys. J.* **84**, 2871 (2003).
- [29] R. Allen, J.-P. Hansen, and S. Melchionna, *Phys. Chem. Chem. Phys.* **3**, 4177 (2001).
- [30] R. Allen, S. Melchionna, and J.-P. Hansen, *Phys. Rev. Lett.* **89**, 175502 (2002).
- [31] R. Allen, S. Melchionna, and J.-P. Hansen, *J. Phys.: Condens. Matter* **15**, S297 (2003).
- [32] R. Allen, J.-P. Hansen, and S. Melchionna, *J. Chem. Phys.* **119**, 3905 (2003).
- [33] R.A. Marcus, *J. Chem. Phys.* **24**, 966 (1956); **24**, 979 (1956).
- [34] B.U. Felderhof, *J. Chem. Phys.* **67**, 493 (1977).
- [35] H. Lowen, J.-P. Hansen, and P.A. Madden, *J. Chem. Phys.* **98**, 3275 (1993).
- [36] D.M. York and M. Karplus, *J. Phys. Chem.* **103**, 11 060 (1999).
- [37] M. Marchi, D. Borgis, N. Levy, and P. Ballone, *J. Chem. Phys.* **114**, 4377 (2001).
- [38] T. HaDuong, S. Phan, M. Marchi, and D. Borgis, *J. Chem. Phys.* **117**, 541 (2002).
- [39] R. Car and M. Parrinello, *Phys. Rev. Lett.* **55**, 2471 (1985).
- [40] P. Attard, *J. Chem. Phys.* **119**, 1365 (2003).
- [41] H. Hoshi, M. Sakurai, Y. Inoue, and R. Chuhˆo, *J. Chem. Phys.* **87**, 1107 (1987).
- [42] C.S. Pomelli, J. Tomasi, and V. Barone, *Theor. Chem. Acc.* **105**, 446 (2001).
- [43] C.S. Pomelli and J. Tomasi, *J. Mol. Struct.: THEOCHEM* **537**, 97 (2001).
- [44] J.D. Jackson, *Classical Electrodynamics*, 3rd ed. (Wiley, New York, 1999).
- [45] Y. Saad and M. Schultz, *SIAM (Soc. Ind. Appl. Math.) J. Sci. Stat. Comput.* **7**, 856 (1986).
- [46] C.T. Kelley, *Iterative Methods for Linear and Nonlinear Equations* (SIAM, Philadelphia, 1995).
- [47] D. Boda, T. Varga, D. Henderson, D.D. Busath, W. Nonner, D. Gillespie, and B. Eisenberg, *Mol. Simul.* **30**, 89 (2004).
- [48] D. Boda, D.D. Busath, D. Henderson, and S. Sokołowski, *J. Phys. Chem. B* **104**, 8903 (2000).
- [49] D. Boda, D. Henderson, and D.D. Busath, *J. Phys. Chem. B* **105**, 11574 (2001).
- [50] D. Boda, D. Henderson, and D.D. Busath, *Mol. Phys.* **100**, 2361 (2002).
- [51] D. Boda, D.D. Busath, B. Eisenberg, D. Henderson, and W. Nonner, *Phys. Chem. Chem. Phys.* **4**, 5154 (2002).
- [52] M. Hoyles, S. Kuyucak, and S.-H. Chung, *Comput. Phys. Commun.* **115**, 45 (1998).